Available online at www.sciencedirect.com
SCIENCE DIRECT®
International Journal of Solids and Structures 42 (2005) 6523–6549
INTERNATIONAL JOURNAL OF SOLIDS and STRUCTURES
www.elsevier.com/locate/ijsolstr

Modeling MEMS resonators with rod-like components accounting for anisotropy, temperature, and strain dependencies

Todd A. Lauderdale *, Oliver M. O'Reilly

Mechanical Engineering, University of California, 2165 Etcheverry Hall, Berkeley, CA 94720, USA

Received 18 May 2004; received in revised form 3 June 2005
Available online 2 August 2005

Abstract

Numerous systems can be described using masses and rods in transverse vibration. Motivated by the desire to model the effects of axial strain and temperature on systems of this type, we develop a procedure to determine the frequencies of transverse vibration of devices composed of rods and rigid masses as functions of these effects. Our models allow for the rods to be composed of anisotropic materials with material symmetry contained in the cubic system. The goal of the present paper is to demonstrate the modeling procedure using the example of a double-ended tuning fork (DETF). Following this, the results of a slightly more complicated model are compared with the experimental results found for a prototype MEMS DETF sensor composed of polycrystalline silicon.

Keywords: MEMS; Cosserat rod; Strain gauge; Silicon

1. Introduction

By way of motivation, one design for a strain sensor is based on the premise that an axial lengthening of a rod will increase its transverse natural frequency. This idea is exploited in double-ended tuning fork (DETF) strain sensors (see Fig. 1). The DETF design was first introduced and patented in the framework of quartz crystal oscillators by EerNisse (1980). Recently, there has been interest in designing microelectromechanical (MEMS) strain sensors using a DETF.

* Corresponding author. Present address: Northrop Grumman, 401 East Hendy Avenue, Sunnyvale, CA 94088, USA. Tel.: +1 650 4941469; fax: +1 510 6435599.
E-mail addresses: toddlauderdale@gmail.com (T.A. Lauderdale), oreilly@me.berkeley.edu (O.M. O'Reilly).

0020-7683/$ - see front matter © 2005 Elsevier Ltd. All rights reserved.
doi:10.1016/j.ijsolstr.2005.06.010

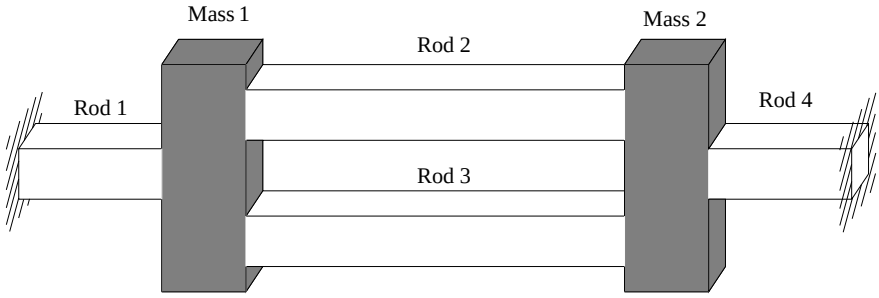

Fig. 1. Schematic of a double ended tuning fork (DETF). This device consists of two central rods (known as tines) which are connected to end masses. The end masses are then attached by rods (known as anchors) to the substrate. Usually, the substrate and DETF are fabricated from the same silicon wafer.

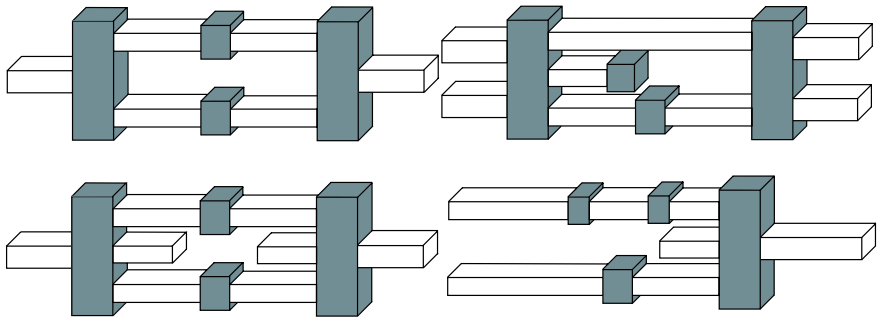

Fig. 2. Four possible resonator designs which the modeling procedure in this paper can accommodate.

Analyzing a silicon MEMS strain sensor which is based on a DETF is non-trivial. First, there is the issue of the anisotropy of the silicon from which the sensor is fabricated. Next, the lateral contraction of the DETF tines induced by the axial strain needs to be considered. Among other issues, there is also the issue of temperature. Most existing models of the DETF are based on the Bernoulli–Euler beam and Timoshenko beam theories and the aforementioned effects are not considered. A finite element model, such as the one used by Beeby et al. (2000) for a MEMS strain gauge, can of course be used, however these models do not provide general design guidelines and can be computationally intensive.

In the present paper, we will develop a model of the transverse vibrations of a DETF composed of crystalline silicon. The model incorporates the end masses, the anisotropy of the silicon, finite deformation effects, and thermal influences and provides a mapping of the transverse resonant frequencies as functions of axial strain and temperature for the DETF. The rods of the DETF are described using a Cosserat rod theory developed by Green, Naghdi and several of their coworkers.[1] The modeling procedure for the DETF can be easily extended to other resonator designs such as those found in Fig. 2, and in fact, we use a similar procedure to model a slightly more complicated model than the basic DETF.

An outline of the paper is as follows. We first provide a brief synopsis of the ideas of Cosserat rod theory important to the present work. This theory is sufficiently general to encompass both Bernoulli–Euler and Timoshenko beam theories, and we use this theory to model the deformation of the system under applied axial strains as well as the transverse deformations of the system. Next, we discuss the free-energy of a rod

[1] The interested reader is referred to the review article (Naghdi, 1982) and the monograph (Rubin, 2000) for references.

composed of a material with cubic symmetry. This section of the paper is primarily based on an earlier work by Green and Naghdi (1979) which we extend by solving the equations for rectangular cross-sections as well as by solving for cubic material with specific crystal orientations. We also relate the constitutive work of Green and Naghdi (1979) to the works of Luo and O'Reilly (2000) and O'Reilly (1998). Also included in this section are prescriptions for, and values of, the Timoshenko shear correction factors and the torsional rigidity of an orthotropic rectangular prismatic rod composed of a material with cubic symmetry.

Next, a model of the axial deformation of the system is developed which includes thermal effects as well as the effects of axial elongation. This model provides the cross-section deformation as well as the internal forces generated by a specific axial extension. To complete the system model, we consider transverse vibration using the Cosserat rod theory. The equations for these vibrations are equivalent to those of a prestressed, anisotropic thermoelastic Timoshenko beam. Finally, we combine the axial and transverse models to determine the natural frequencies of the system as functions of strain and temperature. The results of the basic DETF as well as a comparison between the predicted results of a more complicated model and the experimental results of a prototype MEMS resonant sensor are presented. In the concluding section of the paper, we also present a brief summary of the assumptions used to construct our model.

2. Synopsis of Cosserat rod theory

The Cosserat rod model was developed by Green and Naghdi and co-workers (cf. Green and Naghdi, 1995; Rubin, 2000). It consists of a material curve, $\mathscr{C}$, embedded in Euclidean 3-space. The curve may be parameterized by a single convected coordinate ξ. Associated with each point of this curve are deformable vectors, $\mathbf{d}_\alpha(\xi)$, known as directors which give approximate indications of the deformations of the rod in the planes normal to the curve (for the current analysis, we will consider the case of two directors).[2] The material curve and directors together are known as a Cosserat curve (see Fig. 3). The position of a point on $\mathscr{C}$ is denoted by $\mathbf{r}(\xi)$, and we define

$$\mathbf{d}_3 = \frac{\partial \mathbf{r}}{\partial \xi}, \tag{1}$$

and restrict the motion such that the scalar triple product $[\mathbf{d}_1, \mathbf{d}_2, \mathbf{d}_3] > 0$.

Associated with the Cosserat curve in the present configuration, one can choose a reference configuration such that the material curve is coincidental with the center of area of each cross-section of the undeformed body that the Cosserat curve is modeling. The reference configuration of the Cosserat curve is defined by the vectors $\mathbf{D}_\alpha(\xi)$ and $\mathbf{R}(\xi)$ which are the directors at, and position of, a point in the material curve respectively. As with the current configuration,

$$\mathbf{D}_3 = \frac{\partial \mathbf{R}}{\partial \xi}, \tag{2}$$

and one imposes the restriction $[\mathbf{D}_1, \mathbf{D}_2, \mathbf{D}_3] > 0$. Thus, in the reference configuration we can write the position of a point in the three-dimensional body as

$$\mathbf{R}^* = \mathbf{R}(\xi) + \xi^\alpha \mathbf{D}_\alpha(\xi), \tag{3}$$

where (ξ^1, ξ^2, ξ) are the coordinates of the material point.

For the present configuration, one assumes the following approximation holds

$$\mathbf{r}^* = \mathbf{r} + \xi^\alpha \mathbf{d}_\alpha, \tag{4}$$

[2] In this paper, lower case Greek indices run from 1 to 2, upper case Latin indices run from 1 to 4, and lower case Latin indices run from 1 to 3. We invoke the summation convention on repeated indices unless otherwise noted.

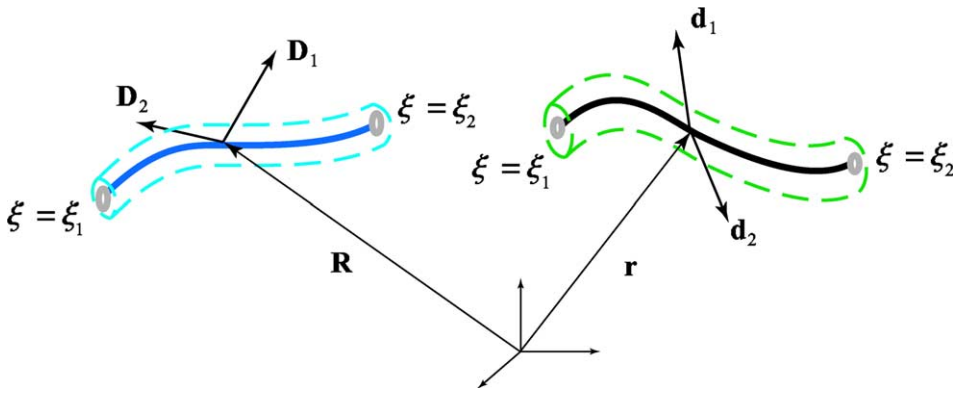

Fig. 3. A schematic depicting the reference and current configurations of a Cosserat rod. The dashed lines represent the lateral surface of the three-dimensional body which the curve is modeling, while the directors $\mathbf{D}_\alpha$ and $\mathbf{d}_\alpha$ and the curves (indicated by the bold lines) comprise the Cosserat rod in the current and reference configurations. In this figure, the material points on the curve $\mathscr{C}$ are distinguished by a coordinate ξ which ranges from $\xi = \xi_1$ to $\xi = \xi_2$.

where **r*** is the position of any particle in the present configuration. To include thermal effects, the temperature in the body is approximated by

$$\theta^* = \theta + \xi^\alpha \theta_\alpha, \tag{5}$$

where $\theta = \theta(\xi, t)$ is the temperature of the body at a point on $\mathscr{C}$ and $\theta_\alpha = \theta_\alpha(\xi, t)$ are temperature fields in the cross-section. From (5), it can be seen that one is assuming a linear variation in temperature across each cross-section. We refer to the temperature along the curve in the reference configuration by Θ, and the reference temperature fields by Θ_α. We then define

$$\begin{aligned} \overline{\theta} &= \theta - \Theta, \\ \overline{\theta}_\alpha &= \theta_\alpha - \Theta_\alpha, \end{aligned} \tag{6}$$

which are the deviations from the reference temperatures.

The following strain measures for a Cosserat rod are used

$$\gamma_{ij} = \mathbf{d}_i \cdot \mathbf{d}_j - \mathbf{D}_i \cdot \mathbf{D}_j, \tag{7}$$

$$\kappa_{\alpha j} = \mathbf{d}'_\alpha \cdot \mathbf{d}_j - \mathbf{D}'_\alpha \cdot \mathbf{D}_j, \tag{8}$$

where $(\,)' = \partial/\partial\xi$. The measures γ_{ij} describe deformations in each cross-section such as a contraction in the $\mathbf{d}_1$ direction, while the measures $\kappa_{\alpha j}$ describe how the deformation varies along the length of the rod such as how the rod is twisting. Using these measures, the free-energy of the rod is

$$\psi = \psi(\gamma_{ij}, \kappa_{\alpha i}, \theta, \theta_\alpha, \mathbf{R}, \mathbf{D}_\alpha, \Theta, \Theta_\alpha). \tag{9}$$

As discussed for the purely mechanical case in Green et al. (1974), this is a properly invariant form of the free-energy for a Cosserat rod.

In the sequel, the body that the Cosserat curve is used to model is assumed to be rod-like. Further, it is assumed that this rod-like body is straight, has a constant rectangular cross-section, and is unstressed in its reference configuration. We also let the vectors $\mathbf{D}_\alpha$ be coincident with the first two vectors, $\mathbf{E}_\alpha$, of an orthonormal triad aligned with the principal axes of the rod's cross-section. That is,

$$\mathbf{D}_1 = \mathbf{E}_1, \quad \mathbf{D}_2 = \mathbf{E}_2, \quad \mathbf{D}_3 = \frac{\partial \mathbf{R}}{\partial \xi} = \mathbf{E}_3, \tag{10}$$

where $\mathbf{E}_3$ lies along the tangent to the curve $\mathscr{C}$. We also assume that the rod is only subject to small deformations, and write

$$\mathbf{r} = \mathbf{R} + \mathbf{u}, \quad \mathbf{d}_i = \mathbf{D}_i + \boldsymbol{\delta}_i, \tag{11}$$

where $\mathbf{u} = u_i\mathbf{E}_i$ and $\boldsymbol{\delta}_i = \delta_{ij}\mathbf{E}_j$. Then linear deformation measures are given by

$$\gamma_{ij} = \delta_{ij} + \delta_{ji}, \quad \kappa_{\alpha i} = \frac{\partial \delta_{\alpha i}}{\partial \xi}, \tag{12}$$

where $\delta_{3i} = \partial u_i/\partial\xi$. The relationships between the six three-dimensional linear strains ϵ_{ik} and the twelve linear Cosserat strain measures are recalled in (B.6) and (B.7). For a homogeneous deformation of the three-dimensional body that the rod is modeling, the following correspondences can be made from these relations: $\gamma_{ik} = \epsilon_{ik}$. Otherwise, some of the strains $\kappa_{\alpha i}$ will be non-zero. These strains, representing torsional (κ_{12} and κ_{12}), flexural (κ_{13} and κ_{23}) and lateral (κ_{11} and κ_{22}) deformations, contribute to the three-dimensional strains in an affine manner.

3. Prescriptions for the constitutive equations

We now turn to prescriptions of the free-energy function for the material and geometries of interest, which are necessary to use the Cosserat theory. In the present paper, we are interested in a thermoelastic free-energy function for a rectangular prismatic rod of a material with symmetry in the cubic system. Examples of material that possess this symmetry are aluminum, diamond, iron, and, as emphasized in the sequel, silicon. We also assume that the axes of the crystal lattice are aligned with the directors in the reference configurations, or, equivalently, that the material has (100) orientation. Thus, the rod is orthotropic.

In the paper Green and Naghdi (1979), the authors developed a free-energy function for circular prismatic rods with orthotropic symmetry. Their development is non-trivial in that they had to compare exact solutions from the Cosserat rod theory to those from linear elasticity in order to determine the values of the various coefficients in the free-energy function.[3] We will extend this work to include rods with rectangular cross-sections (see Fig. 4) and narrow the scope from any orthotropic material to (100) crystalline silicon.

The development of the free-energy function will proceed as follows. First, the symmetry of the rods in the device is discussed. This is addressed in two equivalent manners. For the first approach, we provide the symmetry groups of the rods. This method is based on the treatment in Luo and O'Reilly (2000). The second approach considers the form-invariance of the free-energy function to transformations of the directors. This is the method used in Green and Naghdi (1979). Following our discussion of symmetry, we then proceed, after showing that it is appropriate, by adapting the free-energy function in Green and Naghdi (1979) to the present case by narrowing from any general orthotropic material to (100) cubic crystals and extending from only circular cross-sections to rectangular cross-sections.

3.1. Symmetry group for a rod with cubic symmetry

The symmetry of the material, the geometry of the rod, and the orientation of the crystal lattice with respect to the rod are important factors in reducing the complexity of the Cosserat rod free-energy function. According to Zheng (1994), the least symmetry that any member of the cubic crystal group is subject to is the point group $\mathscr{T}$, given by the following generators:

$$\{\mathbf{R}(2\pi/3, \mathbf{c}), -\mathbf{R}_i\}, \tag{13}$$

[3] O'Reilly (1998) provides a review of the various approaches to this problem for elastic rods.

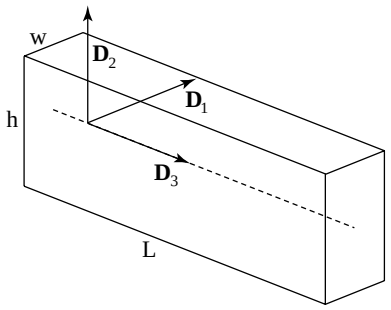

Fig. 4. Schematic of one of the parallelepipeds that will be modeled using a Cosserat rod in this paper. The parallelepiped has a height h, length L and width w. This figure also shows our choice for the referential directors $\mathbf{D}_\alpha$, and the material curve $\mathscr{C}$. The former are taken to be orthonormal and the latter corresponds to the centerline of the parallelepiped. The vector $\mathbf{D}_3$ is identical to the tangent vector to the centerline.

where $\mathbf{R}(\theta,\mathbf{n})$ are rotations of θ degrees about the axis $\mathbf{n}$, $\mathbf{R}_\mathbf{n}$ is a reflection in the plane described by $\mathbf{n}$, and

$$\mathbf{c} = \frac{1}{\sqrt{3}}(\mathbf{E}_1 + \mathbf{E}_2 + \mathbf{E}_3). \tag{14}$$

Our subsequent developments hold for any material with at least the symmetries (13).

Now, consider a rod with rectangular cross-section (as shown in Fig. 4) composed of a material with cubic symmetry and fabricated such that the crystal lattice is oriented in the (100) direction with respect to the rod. With this assumption, we find a subgroup of $\mathscr{T}$ for the (affine) symmetry group $\mathscr{A}_{\mathscr{R}_0}$ of the rod. This group is generated by

$$\{\mathbf{R}(\pi,\mathbf{D}_1), \quad \mathbf{R}(\pi,\mathbf{D}_2), \quad \mathbf{R}(\pi,\mathbf{D}_3), \quad \mathbf{I}, \quad -\mathbf{I}\}, \tag{15}$$

where $\mathbf{I}$ is the identity tensor. Note that if the rod has a square cross-section, one recovers more of the group $\mathscr{T}$. The group,

$$\{\mathbf{R}(\pi/2,\mathbf{D}_1), \quad \mathbf{R}(\pi/2,\mathbf{D}_2), \quad \mathbf{R}(\pi,\mathbf{D}_3), \quad \mathbf{I}, \quad -\mathbf{I}\}, \tag{16}$$

is the affine symmetry group for this case.

For a Cosserat rod whose cross-sections are rectangular, we can express symmetry transformations in terms of the vectors $\mathbf{d}_i$ and $\mathbf{D}_i$. It is easy to see that, for the present case, the transformations

$$\begin{aligned}
&(a)\ \mathbf{D}_1 \to -\mathbf{D}_1, \quad \mathbf{d}_1 \to -\mathbf{d}_1, \quad \mathbf{d}'_1 \to -\mathbf{d}'_1,\\
&(b)\ \mathbf{D}_2 \to -\mathbf{D}_2, \quad \mathbf{d}_2 \to -\mathbf{d}_2, \quad \mathbf{d}'_2 \to -\mathbf{d}'_2,\\
&(c)\ \mathbf{D}_3 \to -\mathbf{D}_3, \quad \mathbf{d}_3 \to -\mathbf{d}_3, \quad \mathbf{d}'_\alpha \to -\mathbf{d}'_\alpha,
\end{aligned} \tag{17}$$

are equivalent to the transformations (15). The transformations (17) were prescribed by Green and Naghdi (1979).[4] Thus, in the subsequent work to find the constitutive coefficients for the rod we can benefit from the results given in Green and Naghdi (1979).

Since we are interested in an example with a MEMS device, we now discuss crystalline silicon in more detail. Silicon crystallizes at standard temperature and pressure in the diamond cubic crystal structure. This structure is represented in Fig. 5. The Schoenflies symbol for the space group of the diamond cubic crystal structure is $\mathscr{O}_h^7$ as given in Bragg and Claringbull (1965). The generators of the related point group $\mathscr{O}_h$ are, from (Zheng, 1994),

[4] Specifically, these are the transformations (a)–(c) given on page 844 of Green and Naghdi (1979). Luo and O'Reilly (2000) have shown how these transformations are accommodated in a treatment of material symmetry based on the group (15).

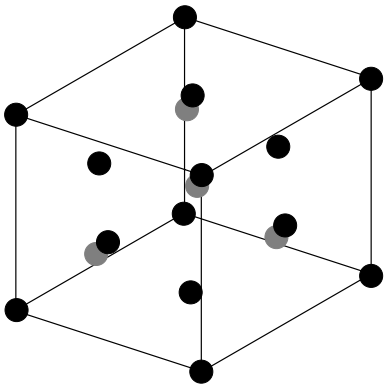

Fig. 5. A unit cell of the diamond cubic crystal structure of crystalline silicon. There is an atom at each corner as well as in the center of each face of the cube (black circles). In addition, there are four other atoms situated in the interior of the cube (gray circles).

$$\left\{\mathbf{R}(2\pi/3,\mathbf{c}),\quad \mathbf{R}(\pi/2,\mathbf{E}_1),\quad \mathbf{R}_{\mathbf{E}_2},\quad -\mathbf{I}\right\}. \tag{18}$$

Crystalline silicon is contained in the cubic system so the forthcoming results pertain to silicon.

3.2. Free-energy function

We now use the symmetries discussed in the previous section to reduce the free-energy function. Using the director transformations (17), Green and Naghdi showed that for a rod with the material and geometric properties of the present work, the free-energy function of a linear thermoelastic rod can be no more complicated than

$$\begin{aligned}2\lambda\psi = {} & k_1\gamma_{11}^2 + k_2\gamma_{22}^2 + k_3\gamma_{33}^2 + k_4\gamma_{21}^2 + k_5\gamma_{23}^2 + k_6\gamma_{13}^2 + k_7\gamma_{11}\gamma_{22} + k_8\gamma_{11}\gamma_{33} + k_9\gamma_{22}\gamma_{33} + k_{10}\kappa_{11}^2 \\ & + k_{11}\kappa_{22}^2 + k_{12}\kappa_{12}^2 + k_{13}\kappa_{21}^2 + k_{14}\kappa_{12}\kappa_{21} + k_{15}\kappa_{23}^2 + k_{16}\kappa_{13}^2 + k_{17}\kappa_{11}\kappa_{22} + k_{18}(\overline{\theta})^2 + k_{19}(\overline{\theta}_1)^2 \\ & + k_{20}(\overline{\theta}_2)^2 + k_{21}\gamma_{11}\overline{\theta} + k_{22}\gamma_{22}\overline{\theta} + k_{23}\gamma_{33}\overline{\theta} + k_{24}\kappa_{13}\overline{\theta}_1 + k_{25}\kappa_{23}\overline{\theta}_2.\end{aligned} \tag{19}$$

A detailed discussion of the reduction from a general quadratic form to the above result is provided in Appendix A.

To use the rod theory, the 25 constitutive coefficients in (19) must be determined. Since the material and geometries in question are a subset of those discussed by Green and Naghdi (1979), we will specialize their results. The first step is to describe the mechanical and thermal properties of the material. We find from Carlson (1972) and Gurtin (1972) that the linear stress–strain–temperature relationship for cubic crystals is,

$$\begin{aligned}\sigma_{ii} &= h_{11}\epsilon_{ii} + h_{12}(\epsilon_{jj} + \epsilon_{kk}) + m_{ii}(\theta^* - \Theta), \quad \text{(no sum on } i,j,k),\\ \sigma_{ij} &= h_{44}(\epsilon_{ij} + \epsilon_{ji}) + m_{ij}(\theta^* - \Theta) \quad (i \neq j).\end{aligned} \tag{20}$$

Here, σ_{ij} are the components of the stress tensor, ϵ_{ij} are the Cartesian components of the infinitesimal strain tensor, m_{ij} are the components of the stress–temperature tensor, and h_{ij} are the components of the elasticity tensor.

The thermal expansion tensor for silicon is

$$\mathbf{A} = \alpha\mathbf{I}, \tag{21}$$

where α is the thermal expansion coefficient. From this tensor, we find the related stress–temperature tensor

$$\mathbf{M} = m\mathbf{I}, \tag{22}$$

where the constant m is given in terms of the thermal expansion coefficient α by[5]

$$m = \alpha(h_{11} + 2h_{12}). \tag{23}$$

It follows that the thermoelastic behavior of the material is characterized by the three elastic coefficients, h_{11}, h_{12} and h_{44}, the thermal expansion coefficient α, and by the specific heat c.

By specifying the results for the free-energy coefficients found in Green and Naghdi (1979) for cubic crystals, and by extending the results to rectangular cross-sections, the following free-energy constants are determined (see Appendix B for a full derivation of these results):

$$\begin{aligned}
&k_1 = k_2 = k_3 = \frac{1}{4}Ah_{11}, \quad k_4 = Ah_{44}, \quad k_5 = k^1 Ah_{44}, \quad k_6 = k^2 Ah_{44}, \quad k_7 = k_8 = k_9 = \frac{1}{2}Ah_{12},\\
&k_{10} = I_{11}h_{12}, \quad k_{11} = I_{22}h_{12}, \quad k_{12} = k_{13} = \frac{1}{4}\mathscr{D} + \frac{1}{2}h_{44}(I_{11} + I_{22}),\\
&k_{14} = h_{44}(I_{11} + I_{22}) - \frac{1}{2}\mathscr{D}, \quad k_{15} = I_{22}\frac{(h_{11} + 2h_{12})(h_{11} - h_{12})}{(h_{11} + h_{12})}, \quad k_{16} = \frac{I_{11}}{I_{22}}k_{15}, \quad k_{17} = 0,\\
&k_{18} = -Ac, \quad k_{19} = \frac{k_{20}I_{11}}{I_{22}}, \quad k_{20} = -I_{22}\left(c + \frac{2\alpha^2}{(h_{11} + h_{12})}\right),\\
&k_{21} = k_{22} = k_{23} = -\alpha A(h_{11} + 2h_{12}), \quad k_{24} = \frac{k_{25}I_{11}}{I_{22}}, \quad k_{25} = -2I_{22}\alpha\left(1 - \frac{2h_{12}}{(h_{11} + h_{12})}\right),
\end{aligned} \tag{24}$$

where

$$A = \int_{A(\xi)} \mathrm{d}A, \quad I_{11} = \int_{A(\xi)} \xi^1\xi^1 \,\mathrm{d}A, \quad I_{22} = \int_{A(\xi)} \xi^2\xi^2 \,\mathrm{d}A. \tag{25}$$

Also, $\mathscr{D}$ is the torsional rigidity, which for an æleotropic prism with rectangular cross-section, is

$$\mathscr{D} = h_{44}wh^3\left(\frac{2}{3} - \frac{128h}{\pi^5 w}\sum_{n=0}^{\infty}\frac{1}{(2n+1)^5}\tanh\frac{(2n+1)\pi w}{2h}\right). \tag{26}$$

This result is taken directly from section 226 of Love (1927).

Finally, in the equations, the coefficients k^1 and k^2 are the shear correction factors—due to anisotropy there are two such coefficients. As described in Appendix B, we solve the boundary-value problems for rectangular cross-sections given by Green and Naghdi (1979) for the values of k^1 and k^2. This solution is found using a procedure similar to that discussed in Love (1927). To elaborate on the factors k^1 and k^2 further, it is convenient to define the function

$$K(r) = \left(\frac{3}{2} + \frac{h_{12}h_{44}r^2}{(h_{11} + 2h_{12})(h_{12} - h_{11})}\left(1 + \frac{12}{\pi^2}\sum_{n=1}^{\infty}\frac{(-1)^n}{n^2}\operatorname{sech}(n\pi r)\right)\right)^{-1}, \tag{27}$$

which is related to Eq. (B.20). With this function, $k^1 = K(w/h)$ and $k^2 = K(h/w)$. Fig. 6 shows the function $K(r)$ with the elastic parameters of crystalline silicon as r is varied. From this figure, it is easy to determine the anisotropic Timoshenko shear correction factors for a rectangular prism of single-crystal silicon. Notice that the correction factor is dependent on the ratio of the rod's height to its width as well as the three elastic

[5] We are using Eq. (7.26) from Carlson (1972) for this identification.

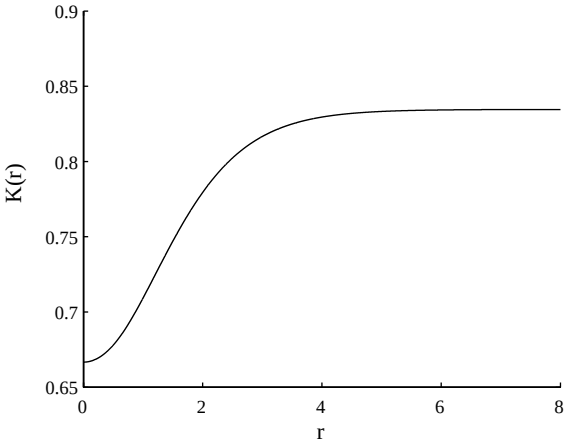

Fig. 6. The function $K(r)$ defined by Eq. (27) for the material properties of silicon. The Timoshenko shear correction factors are $k^1 = K(r)$ and $k^2 = K(1/r)$.

material constants.[6] The values for the shear coefficient range from approximately 0.66–0.83. These values are similar in range to those obtained by Kawashima (1996) and by Hutchinson (2001).

4. Axial deformation model

Since we have determined the constitutive function for a silicon rod, we can now turn to modeling the dynamics of the DETF. The first step in developing the model of the dynamics is to understand the axial deformation of the system. In order to accomplish this, we will use Cosserat rod theory and a slightly simplified approximation of the DETF. Since we are assuming that the two main tines are symmetric, when the device is elongated axially the forces in each tine are equal. Using this knowledge, for the axial deformation case we approximate the DETF as three rods connected by rigid connections. The middle rod's width in the axial model we take to be the sum of the middle tines of the DETF (see Fig. 7). We will then split the force found in the middle rod of the three rod axial solution to find the force in each of the four rods for the dynamic analyses. From this simplified model, we can predict the axial deformation of the full DETF.

The derivation of the governing equations of the axial deformation is similar to that given in Kinkaid and O'Reilly (2002) except the current model includes anisotropy and thermal effects. For each rod in the axial deformation model, we use the free-energy function (19) with finite strain measures and the material constants developed in Section 3.1. Fig. 7 shows a schematic of an axial deformation of the simplified DETF model and the director naming conventions.

4.1. Axial equations

As in Kinkaid and O'Reilly (2002), for each rod we assume an axial extension with cross-sections perpendicular to $\mathscr{C}$ remaining perpendicular. Thus, the motion of rod i is

[6] Puchegger et al. (2003) also recently found a shear coefficient with a dependence on w/h, however we have been unable to compare our results to theirs.

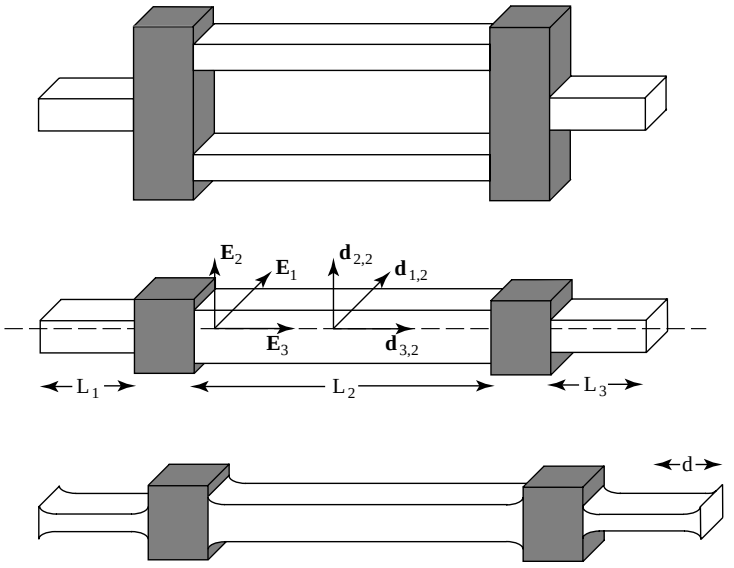

Fig. 7. Cosserat rod schematics showing the DETF, the approximation of the DETF, and the deformed rod subject to an axial elongation of d. Also illustrated is the naming convention for the directors.

$$\begin{aligned}\mathbf{r}_i &= x_i(\xi)\mathbf{E}_3,\\ \mathbf{d}_{1,i} &= d_{1,i}(\xi)\mathbf{E}_1,\\ \mathbf{d}_{2,i} &= d_{2,i}(\xi)\mathbf{E}_2.\end{aligned} \tag{28}$$

That is, the rod stays straight and the vectors $\mathbf{d}_{i,j}$ remain orthogonal and retain their orientation. Consequently, the non-trivial strains are

$$\gamma_{11,i} = d_{1,i}^2 - 1, \quad \gamma_{22,i} = d_{2,i}^2 - 1, \quad \gamma_{33,i} = \left(\frac{\partial x_i}{\partial \xi}\right)^2 - 1, \tag{29}$$

and

$$\kappa_{11,i} = d'_{1,i} d_{1,i}, \quad \kappa_{22,i} = d'_{2,i} d_{2,i}. \tag{30}$$

The strains which are not prescribed in Eqs. (29) and (30) are identically zero.

As in Fig. 7, we let the length of each rod be L_i. We define the following variables to aid in non-dimensionalizing the equilibrium equations:

$$w_i = \frac{x_i - \xi}{L_i}, \quad s_i = \frac{\xi}{L_i}. \tag{31}$$

After following a procedure similar to the one found in Kinkaid and O'Reilly (2002), the differential equations governing the steady state axial deformation of each rod are

$$\begin{aligned}w_i'' = &-(4k_{3,i}(w_i' + 1)^2 + 2k_{3,i}((w_i')^2 + 2w_i') + k_{8,i}\gamma_{11,i} + k_{9,i}\gamma_{22,i}\\ &+ k_{23,i}\overline{\theta}_i)^{-1}(k_{8,i}\gamma'_{11,i} + k_{9,i}\gamma'_{22,i} + k_{23,i}\overline{\theta}'_i)(w_i' + 1),\end{aligned} \tag{32}$$

$$\gamma''_{11,i} = \frac{2L_i^2}{k_{10,i}}(2k_{1,i}\gamma_{11,i} + k_{7,i}\gamma_{22,i} + k_{8,i}((w_i')^2 + 2w_i') + k_{21,i}\overline{\theta}_i), \tag{33}$$

$$\gamma''_{22,i} = \frac{2L_i^2}{k_{11,i}}(2k_{2,i}\gamma_{22,i} + k_{7,i}\gamma_{11,i} + k_{9,i}((w_i')^2 + 2w_i') + k_{22,i}\overline{\theta}_i). \tag{34}$$

In these equations, $()' = \frac{\partial}{\partial s_i}$. In addition to the mechanical equations, there is an equation governing the temperature in the rod, but since we are solving for steady state deformations, this equation is trivially satisfied.

After solving (32)–(34) subject to the appropriate boundary conditions, the axial force in each composite rod is determined using the constitutive relation

$$\mathbf{n}_i = (2k_{3,i}\gamma_{33,i} + k_{8,i}\gamma_{11,i} + k_{9,i}\gamma_{22,i} + k_{23,i}\overline{\theta})\frac{\partial x}{\partial \xi}\mathbf{E}_3. \tag{35}$$

Then, for the middle tines, we assume that the force in each rod is found using the following procedure: we take the ratio of the individual rod's cross-sectional area to the composite rod's cross-sectional area then multiply this ratio with the axial force of the composite rod.

4.2. Continuity and boundary conditions

Given the governing equations, we need to define continuity and boundary conditions to relate the deformations of each individual rod to each other and to the structure as a whole. The connections of one rod to another are approximated as rigid, giving zero lateral strain at the end of each rod:

$$\gamma_{11,i}(0) = 0, \quad \gamma_{11,i}(1) = 0, \quad \gamma_{22,i}(0) = 0, \quad \gamma_{22,i}(1) = 0. \tag{36}$$

Also, at each connection, the deflection of the right end of the left rod is equal to the deflection of the left end of the rod on the right. Therefore,

$$w_2(0) = \frac{L_1}{L_2}w_1(1), \quad w_3(0) = \frac{L_2}{L_3}w_2(1). \tag{37}$$

We will be applying a strain of ϵ to the overall structure. Or, equivalently, moving the right end of the structure a distance of $d = \epsilon(L_1 + L_2 + L_3)$ (note that we are ignoring the length of the rigid connections) and not moving the left end of the structure:

$$\epsilon = \frac{d}{L_1 + L_2 + L_3}. \tag{38}$$

Thus, associated with the overall axial strain ϵ of the structure, we have

$$w_3(1) = \frac{d}{L_3}, \quad w_1(0) = 0. \tag{39}$$

The forces across connections of each rod are equal. This implies that

$$\begin{aligned} w_1'(1) &= \left(\frac{k_{3,2}}{k_{3,1}}(w_2'(0)^2 + 2w_2'(0)) + \frac{k_{23,2}}{2k_{3,1}}\theta_2(0) - \frac{k_{23,1}}{2k_{3,1}}\theta_1(1) + 1\right)^{1/2} - 1, \\ w_2'(1) &= \left(\frac{k_{3,3}}{k_{3,2}}\left(w_3'(0)^2 + 2w_3'(0)\right) + \frac{k_{23,3}}{2k_{3,2}}\theta_3(0) - \frac{k_{23,2}}{2k_{3,2}}\theta_2(1) + 1\right)^{1/2} - 1. \end{aligned} \tag{40}$$

With these boundary and continuity conditions we have a complete set of equations and can solve the system of ordinary differential equations (32)–(34).

4.3. Axial results

We now consider the previous development and solve the boundary-value problem using MATLAB for multiple temperatures and strains to illustrate the utility of our equations.

The first figure, Fig. 8, shows the axial force in the left anchor of the DETF as a function of axial strain for various temperatures. According to the governing equations, the axial force is constant through the composite rod. Since there are two tines that make up the middle rod in the composite rod, the axial force in each tine will be half the force shown in Fig. 8. We have plotted a range of axial strains from -0.1% to 0.1% and three different system temperatures. It is interesting to note that for the strain and temperature ranges in Fig. 8, the axial force is an approximately linear function of strain. Also, note that this figure shows the sensitivity of the device to temperature. According to the plot, a change in temperature of about 100 °C is equivalent to stretching the device about 0.04%.

Fig. 9 shows the axial strain ϵ of the composite rod as a function of the axial position (neglecting the thickness of the rigid masses). The slope changes on the plot at a connection between the middle rod

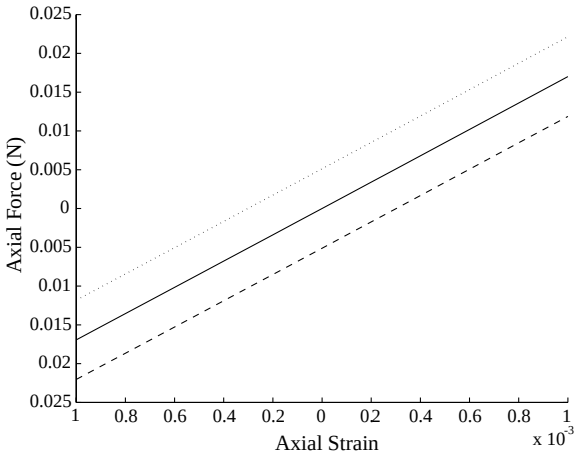

Fig. 8. Axial force $n_{1,3}$ versus axial strain ϵ for three different temperatures for the left anchor rod of a DETF. The dashed line denotes $\overline{\theta} = 100$, the solid line denotes $\overline{\theta} = 0$, and the dotted line denotes $\overline{\theta} = -100$.

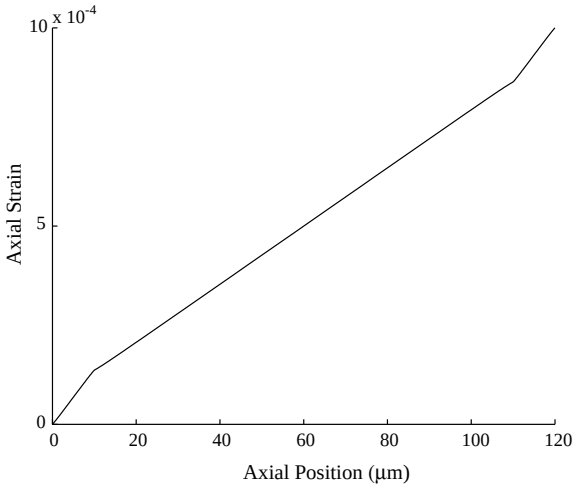

Fig. 9. Axial strain $w/(L_1 + L_2 + L_3)$ as a function of axial position ξ in the composite structure with $\overline{\theta} = 0$. Notice the axial strain in the anchor rods.

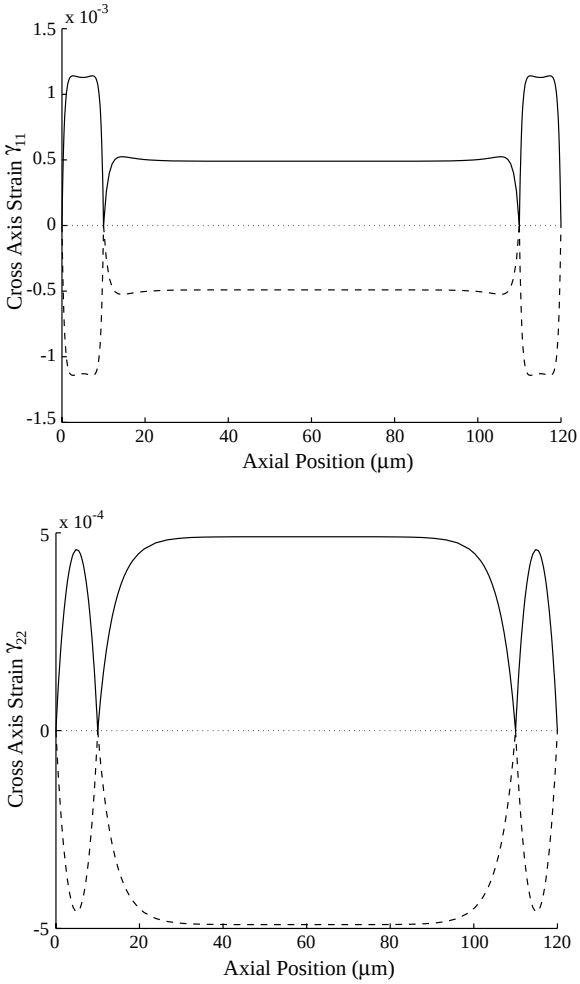

Fig. 10. The lateral strains γ_{11} and γ_{22} for a DETF under axial strain. All solutions are given at the reference temperature, a solid line denotes solutions with -0.1% strain, a dotted line denotes 0% strain, and a dashed line denotes 0.1% strain. The top figure shows the strain γ_{11} for each of the three rods. The bottom figure shows the strain γ_{22} for each of the same three rods.

and each anchor rod. The addition of the anchor rods attenuates the strain felt in the resonating tines and thus, it decreases the sensitivity of the device.

Fig. 10 shows the strains γ_{11} and γ_{22} over the entire length of the rod. There are three different deformations shown in this figure. All of the results are shown at the reference temperature. Notice that for a deformation of $\pm 0.1\%$, the maximum strain is 0.04%, so the effects of the cross-section deformation are minimal. For the rest of the analysis, we will ignore the boundary regions and take the rod dimensions to be those of the center section of the deformed rod.

5. Flexural model

The previous section demonstrated how to quantify the deformation of the system due to axial elongation and thermal variations. This development provides the axial force and deformed geometry of the

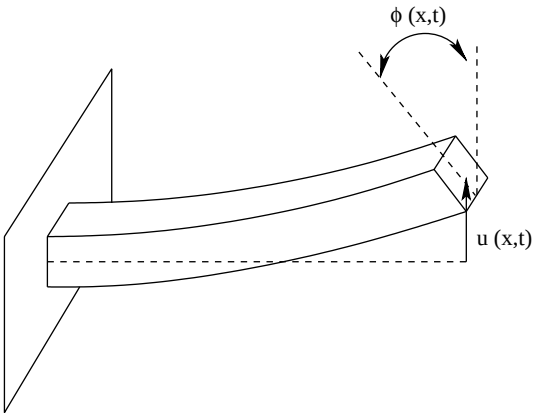

Fig. 11. Schematic of the displacement u and rotation ϕ in the flexural equations of the Cosserat rod theory.

device when given an axial strain and temperature variation. The next step needed to understand the DETF dynamics is to determine its natural frequencies assuming a prescribed axial force. To do this, we will use the flexural equations for a Cosserat rod found in Green and Naghdi (1979). These equations are similar to the Timoshenko equations except the Cosserat equations include the anisotropy of the rod and thermal effects. The solution of the equations gives the transverse displacement of a point of the centerline from its neutral state, $u(x,t)$, and the rotation of the cross-section, $\phi(x,t)$ (see Fig. 11).

In this section of the paper we will develop the governing equations for each rod in the structure. Then, after supplementing these equations by continuity conditions and Euler's laws for a rigid body, we develop a procedure to solve for the natural frequencies of the system.

5.1. Transverse flexural equations

First, we assume that the temperature variation in the rod only occurs along the centerline. That means that $\overline{\theta}_1 = \overline{\theta}_2 = 0$. With this assumption, the governing equations in the $\mathbf{d}_1$ direction, which include the influence of an axial force, are the flexure equations found in Green and Naghdi (1979),

$$k_6\left(\frac{\partial^2 u}{\partial \xi^2} - \frac{\partial \phi}{\partial \xi}\right) + F\frac{\partial^2 u}{\partial \xi^2} = \rho A \frac{\partial^2 u}{\partial t^2}, \tag{41}$$

$$k_{16}\frac{\partial^2 \phi}{\partial \xi^2} + k_6\left(\frac{\partial u}{\partial \xi} - \phi\right) = \rho I l \frac{\partial^2 \phi}{\partial t^2}, \tag{42}$$

where the identifications,

$$\delta_{13} = -\phi, \quad \delta_{31} = \frac{\partial u}{\partial \xi}, \tag{43}$$

are made. Following Rubin (2000), we will define two correction factors; l is a correction factor for the rotary inertia terms and k is a shear correction factor. We take the coefficient k_6 from (24), then multiply by the correction factor such that we obtain a new value for k_6: $k_6 = k k_6$. In addition,

$$V = k_6\left(\frac{\partial u}{\partial \xi} - \phi\right), \quad M = k_{16}\frac{\partial \phi}{\partial \xi}, \tag{44}$$

are the shear force and the bending moment, respectively.

The equation governing the temperature $\overline{\theta}_1$ is

$$-k_{19}\frac{\partial\overline{\theta}_1}{\partial t}+\frac{1}{2}k_{24}\frac{\partial^2\phi}{\partial t\partial\xi}=\rho(s_1+b_2\overline{\theta}_1)-e_1\frac{\partial^2\overline{\theta}_1}{\partial\xi^2}. \tag{45}$$

With our assumptions about the temperature distribution, we can simplify (45) to

$$\frac{1}{2}k_{24}\frac{\partial^2\phi}{\partial t\partial\xi}=\rho s_1. \tag{46}$$

And, given $\phi(x,t)$ we can solve for the required entropy supply ρs_1.

Fig. 4 shows the DETF structure. We will assume the end masses, because of their relative thickness, to be rigid. Thus, the DETF model will be composed of four rods in transverse vibration with two masses internal to the system. The motion of each rod in the system will be governed by Eqs. (41) and (42), so every rod will have a similar form of solution for $u(x,t)$ and $\phi(x,t)$. In the following discussion, quantities associated with each rod will have a subscript of that rod number, i.e., the displacement of rod K will be denoted $u_K(x,t)$. Also, the constitutive coefficient k_i of rod K will be denoted $k_{i,K}$.

In order to make the quantities non-dimensional, we chose the initial dimensions of rod 3 to be reference values. Undeformed quantities will be denoted with an overbar, and the relevant non-dimensional parameters are

$$\eta_K=\frac{L_K}{\overline{L}_3},\quad \delta_K=\frac{h_K}{\overline{L}_3}, \tag{47}$$

$$\tau=t\sqrt{\frac{\overline{k}_{6,3}}{\overline{A}_3\rho(\overline{L}_3)^2}},\quad \zeta_K=\frac{u_K}{\overline{L}_3},\quad s=\frac{\xi}{\overline{L}_3}, \tag{48}$$

$$\alpha_K=\frac{k_{6,K}(\overline{L}_3)^2}{k_{16,K}},\quad \sigma_K=\frac{F_K}{\overline{k}_{6,3}},\quad \eta_K=\frac{k_{6,K}}{\overline{k}_{6,3}},\quad \beta_K=\frac{A_K}{\overline{A}_3}. \tag{49}$$

Using these rod dependent parameters, and substituting into (41) and (42) gives

$$(\sigma_K+\eta_K)\zeta_K''-\eta_K\phi_K'=\beta_K\ddot{\zeta}_K, \tag{50}$$

$$\phi_K''+\alpha_K(\zeta_K'-\phi_K)=\frac{l_K\delta K^2\alpha_K\beta_K}{12\eta_K}\ddot{\phi}_K, \tag{51}$$

where $()'=\frac{\partial}{\partial s}$ and $\dot{()}=\frac{\partial}{\partial\tau}$.

One can combine these two equations into a single fourth-order equation in terms of ϕ_K or ζ_K. Since the equations are separable, let

$$\phi_K(s,\tau)=\phi_K(s)e^{i\Omega\tau},\quad \zeta_K(s,\tau)=\zeta_K(s)e^{i\Omega\tau}. \tag{52}$$

Then one finds the fourth-order ordinary differential equation

$$\phi_K''''+A\phi_K''+B\phi_K=0, \tag{53}$$

for $\phi_K(s)$, where

$$\begin{aligned}A&=(\sigma_K+\eta_K)^{-1}\left[\Omega^2\beta_K+\frac{l_K\delta_K^2\alpha_K\beta_K(\sigma_K+\eta_K)\Omega^2}{12\eta_K}-\alpha_K\sigma_K\right],\\ B&=(\sigma_K+\eta_K)^{-1}\left[\frac{\beta_K^2 l_K\delta_K^2\alpha_K\Omega^4}{12\eta_K}-\alpha_K\beta_K\Omega^2\right].\end{aligned} \tag{54}$$

The solution of this fourth-order homogeneous ordinary differential equation is found by assuming $\phi_K(s) = e^{\lambda_K s}$. This gives an equation for λ_K, the solution of which is

$$\lambda_K = \pm\sqrt{\frac{-A \pm \sqrt{A^2 - 4B}}{2}}. \tag{55}$$

There are three possible forms of the solution to (53) depending on whether λ_K is imaginary or not. Looking at λ_K as a function of Ω we find a non-dimensional cutoff frequency for each rod,

$$\Omega^2_{\mathrm{co}K} = \frac{12\eta_K}{l\beta_K\delta_K^2}, \tag{56}$$

above which λ_K is always imaginary. Thus, as discussed by O'Reilly and Turcotte (1996) there are three distinct regimes for each rod, $\Omega < \Omega_{\mathrm{co}K}$, $\Omega = \Omega_{\mathrm{co}K}$, and $\Omega > \Omega_{\mathrm{co}K}$. Since the structure is composed of 4 rods, there are 12 different possible regimes of oscillation for the DETF composite structure.

Assuming the frequency Ω is below the lowest cutoff frequency of the structure, the solution of (53) is

$$\phi_K(s) = c_{K1}\cos(\lambda_{K1}s) + c_{K2}\sin(\lambda_{K1}s) + c_{K3}\cosh(\lambda_{K2}s) + c_{K4}\sinh(\lambda_{K2}s), \tag{57}$$

where

$$\lambda_{K1} = \sqrt{\frac{A + \sqrt{A^2 - 4B}}{2}}, \quad \lambda_{K2} = \sqrt{\frac{-A + \sqrt{A^2 - 4B}}{2}}. \tag{58}$$

We also find,

$$\zeta_K(s) = a_{K1}\cos(\lambda_{K1}s) + a_{K2}\sin(\lambda_{K1}s) + a_{K3}\cosh(\lambda_{K2}s) + a_{K4}\sinh(\lambda_{K2}s). \tag{59}$$

This solution is found in a straightforward manner from the solution for ϕ_K.

Noticing that $\phi_K(s,\tau)$ and $\zeta_K(s,\tau)$ must satisfy (50) one finds the following familiar relationships:

$$\begin{aligned}
a_{K1} &= \left(\frac{\eta_K\lambda_{K1}}{\beta_K\Omega^2 - (\sigma_K + \eta_K)\lambda_{K1}^2}\right)c_{K2},\\
a_{K2} &= \left(\frac{-\eta_K\lambda_{K1}}{\beta_K\Omega^2 - (\sigma_K + \eta_K)\lambda_{K1}^2}\right)c_{K1},\\
a_{K3} &= \left(\frac{\eta_K\lambda_{K1}}{\beta_K\Omega^2 + (\sigma_K + \eta_K)\lambda_{K1}^2}\right)c_{K4},\\
a_{K4} &= \left(\frac{\eta_K\lambda_{K1}}{\beta_K\Omega^2 + (\sigma_K + \eta_K)\lambda_{K1}^2}\right)c_{K3},
\end{aligned} \tag{60}$$

relating the constants c_{KJ} and a_{KJ}.

Thus, we know the form of the solution for each rod. In the composite structure, the equations are related to each other through continuity conditions. It is to defining these that we now turn.

5.2. Continuity and boundary conditions

The displacement and rotation fields for the four rods are not independent, rather they are linked through continuity equations. That is, the displacements and angles across any joint must be equal, and the forces and moments must be equal in magnitude and opposite in direction (e.g., see Fig. 12). These con-

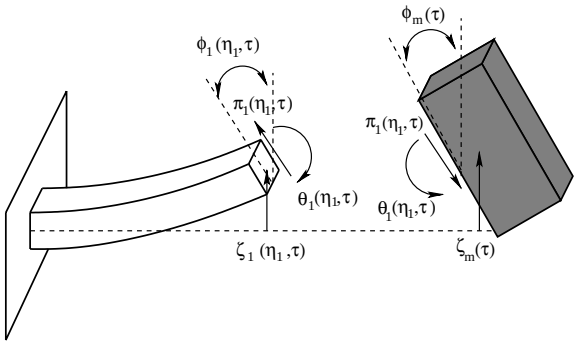

Fig. 12. Continuity at the connection between rod 1 and the rigid body of mass m_1.

tinuity equations as well as the boundary conditions for the system, will provide a complete model for the motion of the composite structure. We now derive these continuity equations.

The linearized angle and displacement continuity equations for each rod in the system are, for rod 1,

$$\zeta_1(\eta_1,\tau) = \zeta_{m1} - \frac{\eta_{m1}}{2}\phi_1(\eta_1,\tau), \quad \phi_1(\eta_1,\tau) = \phi_{m1}, \tag{61}$$

for rod 2,

$$\begin{aligned} \zeta_2(0,\tau) &= \zeta_{m1} + \frac{\eta_{m1}}{2}\phi_{m1}, \quad \phi_2(0,\tau) = \phi_{m1}, \\ \zeta_2(\eta_2,\tau) &= \zeta_{m2} - \frac{\eta_{m2}}{2}\phi_{m2}, \quad \phi_2(\eta_2,\tau) = \phi_{m2}, \end{aligned} \tag{62}$$

for rod 3,

$$\begin{aligned} \zeta_3(0,\tau) &= \zeta_{m1} + \frac{\eta_{m1}}{2}\phi_{m1}, \quad \phi_3(0,\tau) = \phi_{m1}, \\ \zeta_3(\eta_3,\tau) &= \zeta_{m2} - \frac{\eta_{m2}}{2}\phi_{m2}, \quad \phi_3(\eta_3,\tau) = \phi_{m2}, \end{aligned} \tag{63}$$

and for rod 4,

$$\zeta_4(0,\tau) = \zeta_{m2} + \frac{\eta_{m2}}{2}\phi_{m2}, \quad \phi_4(0,\tau) = \phi_{m2}. \tag{64}$$

Here, ϕ_{m1} and ζ_{m1} are the angle and displacement of mass 1, and ϕ_{m2} and ζ_{m2} are the angle and displacement of mass 2. Also,

$$\eta_{m1} = \frac{L_{m1}}{\overline{L}_3}, \quad \eta_{m2} = \frac{L_{m2}}{\overline{L}_3}. \tag{65}$$

Note that each rod's axial coordinate ξ, and therefore s, starts at zero at the left end of the rod. This allows for cleaner notation as well as a reduction in the numerical values of the hyperbolic functions in the equations.

As we did with the other non-dimensional parameters, we use the properties of the undeformed third rod to non-dimensionalize the forces and moments (44). We find

$$\begin{aligned} \pi_K(s,\tau) &= \frac{V_K(s,\tau)}{\overline{k}_{6,3}} = \eta_K(\zeta_K' - \phi), \\ \theta_K(s,\tau) &= \frac{M_K(s,\tau)}{\overline{k}_{6,3}\overline{L}_3} = \frac{\eta_K}{\alpha_K}\phi'. \end{aligned} \tag{66}$$

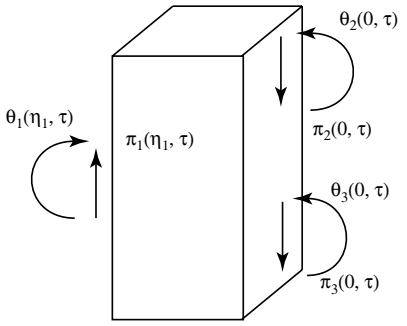

Fig. 13. Forces π and moments θ acting on mass 1.

We will look at the two end masses and write a non-dimensional form of Euler's laws for their motion (see Fig. 13). We find for mass one,

$$\begin{aligned}
&\left(\frac{m_{m1}}{\overline{A}_3\rho\overline{L}_3}\right)\ddot{\zeta}_{m1}(\tau) = \pi_1(\eta_1,\tau) - \pi_2(0,\tau) - \pi_3(0,\tau),\\
&\left(\frac{J_{m1}}{\overline{A}_3\rho\overline{L}_3^3}\right)\ddot{\phi}_{m1}(\tau) = \frac{\eta_{m1}}{2}(-\pi_1(\eta_1,\tau) - \pi_2(0,\tau) - \pi_3(0,\tau)) + \theta_2(0,\tau) + \theta_3(0,\tau) - \theta_1(\eta_1,\tau).
\end{aligned} \tag{67}$$

And we find that

$$\begin{aligned}
&\left(\frac{m_{m2}}{\overline{A}_3\rho\overline{L}_3}\right)\ddot{\zeta}_{m2}(\tau) = \pi_2(\eta_2,\tau) + \pi_3(\eta_3,\tau) - \pi_4(0,\tau),\\
&\left(\frac{J_{m2}}{\overline{A}_3\rho\overline{L}_3^3}\right)\ddot{\phi}_{m2}(\tau) = \frac{\eta_{m2}}{2}(-\pi_2(\eta_2,\tau) - \pi_3(\eta_3,\tau) - \pi_4(0,\tau)) + \theta_4(0,\tau) - \theta_2(\eta_2,\tau) - \theta_3(\eta_3,\tau),
\end{aligned} \tag{68}$$

for mass 2 where $J_{m\alpha}$ is the mass moment of inertia about out-of-plane axis.

The final equations of the flexural model are the boundary conditions. We assume the system to be fixed at both ends, so the boundary conditions become

$$\begin{aligned}
&\zeta_1(0,\tau) = 0,\\
&\phi_1(0,\tau) = 0,\\
&\zeta_4(\eta_4,\tau) = 0,\\
&\phi_4(\eta_4,\tau) = 0.
\end{aligned} \tag{69}$$

Assuming a known axial force and with these boundary conditions, the continuity equations, and the equations for the forces and moments discussed previously, there are a total of 32 equations. In these equations there are the following unknowns: 16 constants a_{KJ}, 6 forces $\pi_K(s,\tau)$, 6 moments $\theta_K(s,\tau)$, 2 displacements $\zeta_{m\alpha}$, 2 angles $\phi_{m\alpha}$, and the frequency Ω. Thus, we can form a homogeneous linear system in terms of the a_{KJ} and Ω.

Let $\mathbf{a} = (a_{11}, a_{12}, \ldots, a_{43}, a_{44})^{\mathrm{T}}$. Then, using Eqs. (62), (63), (67) and (68) and including the values of the unknown constants in terms of the a_{KJ}, we can form a 16×16 matrix, $D(\Omega,\epsilon)$, such that,

$$\mathbf{D}(\Omega,\epsilon)\mathbf{a} = \mathbf{0}. \tag{70}$$

For a non-trivial solution to Eq. (70), one solves for Ω and ϵ for which

$$\det(\mathbf{D}(\Omega, \epsilon)) = 0. \tag{71}$$

The mode shapes of the structures can then be determined by providing values of Ω and ϵ such that $\det(D) = 0$, and then finding a vector in the null space of $\mathbf{D}$. This vector provides the coefficients a_{KJ} to form the mode shape. These computations were all accomplished using MATLAB.

6. Combining the models and results

Using the flexural model, we now know the relationship between the natural frequencies and the axial force. At this point, we can combine the two models. We will take a certain strain and temperature and use the axial model to predict the axial force and the post-deformation dimensions of the rod. We will then use this force and these dimensions to calculate the natural frequencies from the bending model.

6.1. DETF results

We now provide a characterization of the natural frequencies of a specific DETF geometry as a function of strain. Fig. 14(a) shows the first eight natural frequencies of the DETF as functions of strain ϵ ranging from -0.4% to 0.4%. Notice that when the curve characterizing a mode reaches zero natural frequency, the device has buckled. This is an important design consideration, because the device must function through the entire range of strains that one desires to measure. Also shown in this figure is a mode crossing of the sixth and seventh modes. This crossing is not surprising since the device is sufficiently complex, but an effective resonator design will pick device geometries such that these mode crossings do not occur in the range of operation of the device. Fig. 14(b) gives a closer view of the first two natural frequencies with strain varying from -0.1% to 0.1%. From this plot, we can estimate the sensitivity of the device to strain.

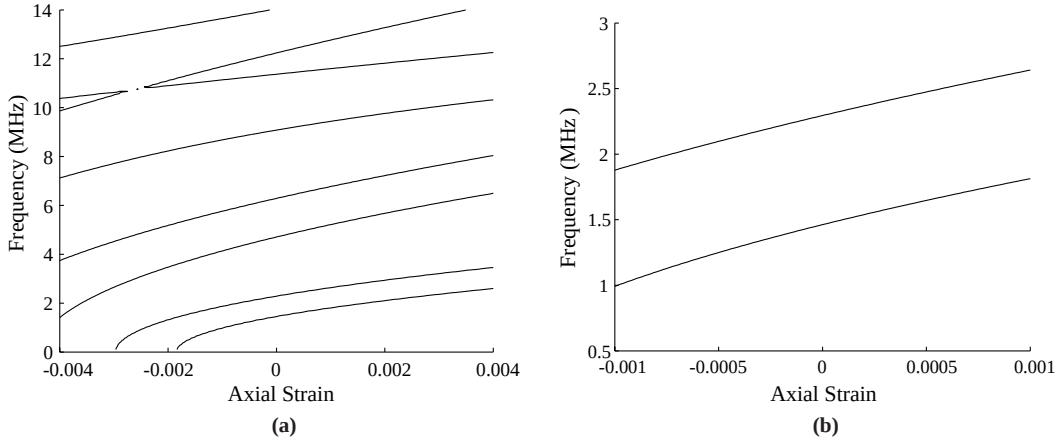

Fig. 14. (a) Resonant frequencies as functions of strain ϵ for a DETF with 100 μm long main tines, 3 μm long anchors, 3 μm rod widths, and 20 μm rod depths. (b) A closer view of the first two modes of the strain response of the same DETF.

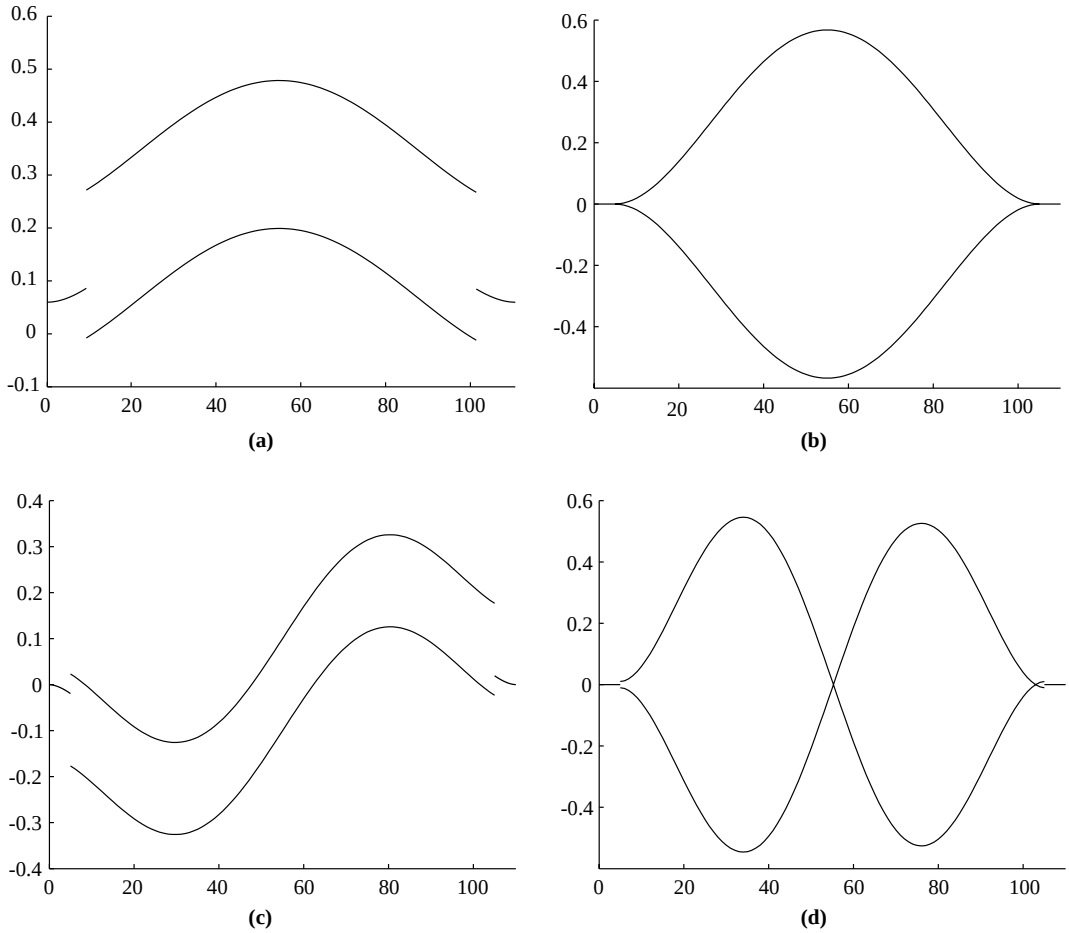

Fig. 15. First four modes for an unstretched DETF. (a) The first mode of vibration occurs at 1.46 MHz. (b) The second mode occurs at 2.54 MHz. (c) The third mode occurs at 5.01 MHz. (d) The fourth mode occurs at 6.96 MHz. The horizontal axis in these four figures shows the axial position in μm.

To further illustrate how the DETF oscillates, Fig. 15 shows the first four mode shapes of the DETF subject to zero strain and a temperature equal to the reference temperature.[7] Note the similar nature of modes 1 and 2 and of modes 3 and 4. These modes are the same for the two main rods, except they are vibrating 180° out of phase. In the second and fourth modes, the vibrations of the two main rods balance each other and there is no motion of the support structure. In the first and third modes, this is not the case, and the vibration of the supports lowers the natural frequency of the system. Depending on the geometry of the supports, the frequencies of modes 1 and 2 may be very similar, so attention must be paid to their design.

Finally, in order to understand the importance of including the material anisotropy in the equations, Fig. 16 shows a comparison of anisotropic results to those obtained using the isotropic approximation of the properties of silicon found in George (1999). The predicted frequency–stress curves differ widely in the two cases, especially as the operating frequency gets higher. Also, the predicted strain sensitivities of the device differ. Using the anisotropic constitutive equations, the predicted sensitivity around zero strain

[7] For modes one and three the anchor rods are not half way between the two tines because of the rotation of the masses.

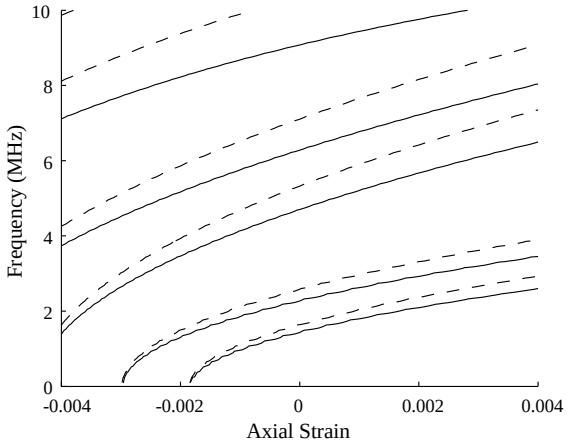

Fig. 16. Comparison of the resonant frequencies as functions of axial strain ϵ for a DETF. The solid line indicates the results including anisotropy, while the dashed line indicates the results obtained using an isotropic approximation.

for the second mode is 348 Hertz per microstrain, but using the isotropic approximation the predicted sensitivity is 409 Hertz per microstrain. Predicting the correct sensitivity is crucial to the design and operation of a strain sensor.

6.2. Prototype device

We will now use the same modeling procedure to understand the dynamics of a slightly more complicated structure. We compare our model to a polycrystalline silicon DETF with a comb drive actuator (see Fig. 17) fabricated and tested with results given in Wojciechowski et al. (2004). To simulate the dynamics, we model the comb drive as a mass located in the middle of the main tines which gives six rods and four masses. By measuring the size of the comb drive we find that each is approximately 30 times as massive as one of the rods adjacent to it. We then use this value for the mass ratio such as that found in $(67)_1$. Likewise, we compute the inertia ratio found in $(67)_2$.

By way of comparison, according to Wojciechowski et al. (2004), the device resonated at 217 kHz which was the frequency that the model predicted. Also, the measured strain sensitivity of the device was 39 Hz/$\mu\epsilon$, while the model predicted a strain sensitivity of 34 Hz/$\mu\epsilon$. When testing the thermal sensitivity of the

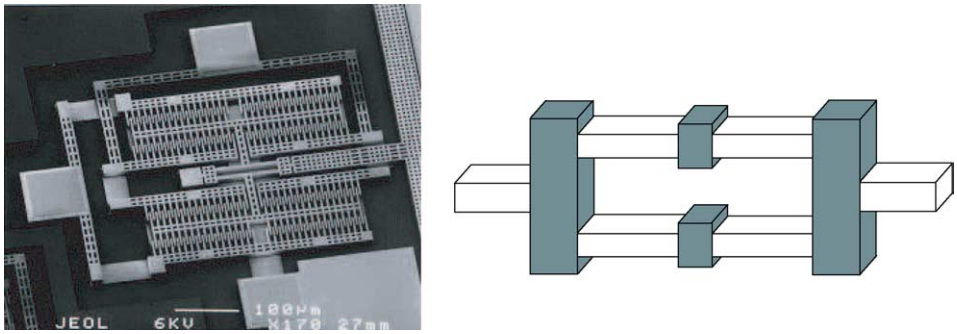

Fig. 17. SEM of the prototype DETF with comb drive actuators and a schematic of the model where we approximate the comb drives with rigid masses.

device, the device was isolated from its surroundings, so there are no stresses due to thermal expansion. Rather, the changes in the material properties with temperature were the main contributers to the thermal sensitivity. With this in mind, the thermal sensitivity of the device was -7 Hz/°C while the model predicted a thermal sensitivity of about -8 Hz/°C. If we assume the anchors of the device do not allow expansion with temperature, the model predicts that the thermal sensitivity is -101 Hz/°C. Thus, according to the model, a device in which the DETF is attached to a substrate will have an actual thermal sensitivity somewhere between -8 Hz/°C and -101 Hz/°C.

7. Concluding remarks

It is prudent to recall the assumptions employed to develop the models for the DETF in Section 6. In particular, we assume that the device consists of a series of rods connected by masses. The undeformed rods are assumed to be straight, prismatic, linearly elastic and have rectangular cross-sections. As discussed in Section 3.1, we assume that the material symmetry of the material that composes these rods is compatible with their geometry. In operational mode, the axial deformation, distributed evenly throughout the rods, is analyzed prior to determining the flexural modes of vibration (i.e, we perform a small-on-large analysis). The flexural modes of vibration feature transverse shear and the equations of motion are similar to those for a Timoshenko beam. Finally, we model the temperature field in the device using the approximation (5). As a consequence of our assumption on the axial deformation, and in spite of the anisotropy of the rods, a sufficient amount of the material symmetry of the rods are preserved to ensure that the (small) flexural vibrations are uncoupled from torsional and extensional vibrations. This feature is a key to the feasibility of our model.

In closing, we have developed and discussed a rod-based model for resonant MEMS devices. This model encompasses many of the geometric and material features which are unique to silicon-based resonators, and is a significant extension to existing models for these devices. Using the model, we have characterized a specific device and predicted the mechanical sensitivity to within 13% of its measured value. As mentioned, our model and the methods we employ can be used to analyze a variety of models and hopefully provide a helpful design tool.

Acknowledgements

Todd Lauderdale was partially supported by a GAANN fellowship from the US Department of Education. Both authors were also partially supported by grant number DAAD-19-02-1-0198 from the US Army Research Office. They are also grateful to B. Boser, A.P. Pisano, and K.E. Wojciechowski for several helpful discussions and for providing us with their experimental data, and to the constructive comments of an anonymous reviewer.

Appendix A. Reduction of the free energy quadratic

The material and geometric symmetries of the rod that were discussed in Section 3.1 allow for simplifications to be made to a general quadratic form of the free energy function. In this appendix, these simplifications are discussed.

We begin by assuming that the free energy function is a quadratic function of its parameters, γ_{ij}, $\kappa_{\alpha i}$, $\overline{\theta}_{\alpha}$, and $\overline{\theta}$. Since there are 15 of these parameters, the quadratic function has 120 terms, which we decompose into 4 sets:

$$\lambda\psi = \lambda\psi_1 + \lambda\psi_2 + \lambda\psi_3 + \lambda\psi_4. \tag{A.1}$$

We will see that the symmetries implied by (17) or equivalently by the group (15) allow us to simplify the constitutive equations by removing terms from (A.1)

We take for the first term of the free energy function, $\lambda\,\psi_1$,

$$\begin{aligned}2\lambda\psi_1 = {} & k_1\gamma_{11}^2 + k_2\gamma_{22}^2 + k_3\gamma_{33}^2 + k_4\gamma_{21}^2 + k_5\gamma_{23}^2 + k_6\gamma_{13}^2 + k_7\gamma_{11}\gamma_{22} + k_8\gamma_{11}\gamma_{33} + k_9\gamma_{22}\gamma_{33} + k_{10}\kappa_{11}^2 \\ & + k_{11}\kappa_{22}^2 + k_{12}\kappa_{12}^2 + k_{13}\kappa_{21}^2 + k_{14}\kappa_{12}\kappa_{21} + k_{15}\kappa_{23}^2 + k_{16}\kappa_{13}^2 + k_{17}\kappa_{11}\kappa_{22} + k_{18}(\overline{\theta})^2 + k_{19}(\overline{\theta}_1)^2 \\ & + k_{20}(\overline{\theta}_2)^2 + k_{21}\gamma_{11}\overline{\theta} + k_{22}\gamma_{22}\overline{\theta} + k_{23}\gamma_{33}\overline{\theta} + k_{24}\kappa_{13}\overline{\theta}_1 + k_{25}\kappa_{23}\overline{\theta}_2. \end{aligned} \tag{A.2}$$

For the second term, $\lambda\psi_2$, we take

$$\begin{aligned}2\lambda\psi_2 = {} & k_{69}\gamma_{11}\gamma_{12} + k_{79}\gamma_{11}\gamma_{13} + k_{115}\gamma_{12}\gamma_{22} + k_{58}\gamma_{12}\gamma_{23} + k_{76}\gamma_{12}\gamma_{33} + k_{73}\gamma_{13}\gamma_{22} + k_{66}\gamma_{13}\gamma_{23} \\ & + k_{78}\gamma_{13}\gamma_{33} + k_{104}\gamma_{11}\kappa_{12} + k_{114}\gamma_{11}\kappa_{13} + k_{26}\gamma_{11}\kappa_{21} + k_{28}\gamma_{12}\kappa_{11} + k_{32}\gamma_{12}\kappa_{22} + k_{33}\gamma_{12}\kappa_{23} \\ & + k_{34}\gamma_{13}\kappa_{11} + k_{38}\gamma_{13}\kappa_{22} + k_{39}\gamma_{13}\kappa_{23} + k_{41}\gamma_{22}\kappa_{12} + k_{42}\gamma_{22}\kappa_{13} + k_{43}\gamma_{22}\kappa_{21} + k_{47}\gamma_{23}\kappa_{12} \\ & + k_{48}\gamma_{23}\kappa_{13} + k_{49}\gamma_{23}\kappa_{21} + k_{53}\gamma_{33}\kappa_{12} + k_{54}\gamma_{33}\kappa_{13} + k_{55}\gamma_{33}\kappa_{21} + k_{59}\kappa_{11}\kappa_{12} + k_{60}\kappa_{11}\kappa_{13} \\ & + k_{61}\kappa_{11}\kappa_{21} + k_{67}\kappa_{12}\kappa_{22} + k_{68}\kappa_{12}\kappa_{23} + k_{71}\kappa_{13}\kappa_{22} + k_{72}\kappa_{13}\kappa_{23} + k_{74}\kappa_{21}\kappa_{22} + k_{75}\kappa_{21}\kappa_{23} \\ & + k_{80}\gamma_{11}\overline{\theta}_1 + k_{82}\gamma_{12}\overline{\theta} + k_{84}\gamma_{12}\overline{\theta}_2 + k_{85}\gamma_{13}\overline{\theta} + k_{87}\gamma_{13}\overline{\theta}_2 + k_{89}\gamma_{22}\overline{\theta}_1 + k_{92}\gamma_{23}\overline{\theta}_1 + k_{95}\gamma_{33}\overline{\theta}_1 \\ & + k_{98}\kappa_{11}\overline{\theta}_1 + k_{100}\kappa_{12}\overline{\theta} + k_{102}\kappa_{12}\overline{\theta}_2 + k_{103}\kappa_{13}\overline{\theta} + k_{105}\kappa_{13}\overline{\theta}_2 + k_{106}\kappa_{21}\overline{\theta} + k_{108}\kappa_{21}\overline{\theta}_2 \\ & + k_{110}\kappa_{22}\overline{\theta}_1 + k_{113}\kappa_{23}\overline{\theta}_1 + k_{116}\overline{\theta\theta}_1 + k_{119}\overline{\theta}_1\overline{\theta}_2. \end{aligned} \tag{A.3}$$

We set

$$\begin{aligned}2\lambda\psi_3 = {} & k_{118}\gamma_{11}\gamma_{23} + k_{64}\gamma_{12}\gamma_{13} + k_{63}\gamma_{22}\gamma_{23} + k_{120}\gamma_{23}\gamma_{33} + k_{27}\gamma_{11}\kappa_{23} + k_{30}\gamma_{12}\kappa_{13} + k_{35}\gamma_{13}\kappa_{12} \\ & + k_{37}\gamma_{13}\kappa_{21} + k_{45}\gamma_{22}\kappa_{23} + k_{46}\gamma_{23}\kappa_{11} + k_{50}\gamma_{23}\kappa_{22} + k_{57}\gamma_{33}\kappa_{23} + k_{62}\kappa_{11}\kappa_{23} + k_{65}\kappa_{12}\kappa_{13} \\ & + k_{70}\kappa_{13}\kappa_{21} + k_{77}\kappa_{22}\kappa_{23} + k_{81}\gamma_{11}\overline{\theta}_2 + k_{83}\gamma_{12}\overline{\theta}_1 + k_{90}\gamma_{22}\overline{\theta}_2 + k_{91}\gamma_{23}\overline{\theta} + k_{99}\kappa_{11}\overline{\theta}_2 + k_{101}\kappa_{12}\overline{\theta}_1 \\ & + k_{107}\kappa_{21}\overline{\theta}_1 + k_{111}\kappa_{22}\overline{\theta}_2 + k_{112}\kappa_{23}\overline{\theta} + k_{117}\overline{\theta\theta}_2. \end{aligned} \tag{A.4}$$

Finally, for $\lambda\psi_4$, we have

$$\begin{aligned}2\lambda\psi_4 = {} & k_{88}\gamma_{11}\kappa_{11} + k_{94}\gamma_{11}\kappa_{22} + k_{29}\gamma_{12}\kappa_{12} + k_{31}\gamma_{12}\kappa_{21} + k_{36}\gamma_{13}\kappa_{13} + k_{40}\gamma_{22}\kappa_{11} + k_{44}\gamma_{22}\kappa_{22} \\ & + k_{51}\gamma_{23}\kappa_{23} + k_{52}\gamma_{33}\kappa_{11} + k_{56}\gamma_{33}\kappa_{22} + k_{86}\gamma_{13}\overline{\theta}_1 + k_{93}\gamma_{23}\overline{\theta}_2 + k_{97}\kappa_{11}\overline{\theta} + k_{109}\kappa_{22}\overline{\theta}. \end{aligned} \tag{A.5}$$

Still following Green and Naghdi (1979), we look at transformations of γ_{ij}, $\kappa_{\alpha i}$, $\overline{\theta}$, and $\overline{\theta}_\alpha$ that are equivalent to (17). For the first group of transformations, $(17)_1$, we find that

$$\begin{aligned}&\gamma_{12} \to -\gamma_{12}, \quad \gamma_{13} \to -\gamma_{13}, \quad \kappa_{12} \to -\kappa_{12}, \\ &\kappa_{21} \to -\kappa_{21}, \quad \kappa_{13} \to -\kappa_{13}, \quad \overline{\theta}_1 \to -\overline{\theta}_1. \end{aligned} \tag{A.6}$$

Since the strain measures and temperatures are independent, these imply that the strain energy function cannot depend on any of the terms in (A.3).

For the second group of transformations, $(17)_2$, we find that

$$\begin{aligned}&\gamma_{12} \to -\gamma_{12}, \quad \gamma_{23} \to -\gamma_{23}, \quad \kappa_{12} \to -\kappa_{12}, \\ &\kappa_{21} \to -\kappa_{21}, \quad \kappa_{23} \to -\kappa_{23}, \quad \overline{\theta}_2 \to -\overline{\theta}_2. \end{aligned} \tag{A.7}$$

Again, since the strain measures and temperatures are independent, these imply that the strain energy function cannot depend on any of the terms in (A.4).

Finally, for the third group of transformations, $(17)_3$, we find that

$$\begin{aligned} &\gamma_{13} \rightarrow -\gamma_{13}, \quad \gamma_{23} \rightarrow -\gamma_{23}, \quad \kappa_{11} \rightarrow -\kappa_{11}, \\ &\kappa_{12} \rightarrow -\kappa_{12}, \quad \kappa_{21} \rightarrow -\kappa_{21}, \quad \kappa_{22} \rightarrow -\kappa_{22}. \end{aligned} \tag{A.8}$$

Thus, the free energy function cannot depend on any of the terms in (A.5). The only terms in the overall quadratic that a rod with the symmetries (17) may depend on are the 25 terms in (A.2). For a different order of application of the symmetries (17), we will find the same result, but the groups (A.3)–(A.5) will be slightly different.

Appendix B. Determining the material constants for a linearly elastic rod

In this appendix, we elaborate on the prescriptions of the 25 k_i in the constitutive equation (19). We first compare the relations (20) to the usual mechanical stress strain relation

$$\sigma_{ij} = c_{ijkl}\epsilon_{kl} + M_{ii}(\theta^* - \Theta), \tag{B.1}$$

to determine the constants c_{ijkl} in terms of h_{11}, h_{12}, and h_{44}. With some work, we find that

$$\begin{aligned} &c_{1111} = c_{2222} = c_{3333} = h_{11}, \\ &c_{1122} = c_{1133} = c_{2233} = h_{12}, \\ &c_{1212} = c_{1313} = c_{2323} = h_{44}. \end{aligned} \tag{B.2}$$

Using these relations, we can write the free-energy function for a three-dimensional linearly elastic solid composed of a material with cubic symmetry. This is

$$\rho_o^*\psi^* = \frac{1}{2}c_{ijkl}\epsilon_{ij}\epsilon_{kl} - m_{ij}\epsilon_{ij}\theta^* - \frac{1}{2}c\theta^{*2} - \rho_o^*\eta_o\theta^*, \tag{B.3}$$

where m_{ij} are the components of the stress–temperature tensor given by (23), c is the specific heat of the material, and η_o is the entropy in the reference state. We assume that $\eta_o = 0$ for the current analysis.

Now, we will use direct integration to determine some of the 25 coefficients, k_i, of the free-energy function. This method, as discussed in O'Reilly (1998), will hold for all deformations such that the approximation

$$\mathbf{r}^*(\xi^1, \xi^2, \xi, t) = \mathbf{r}(\xi, t) + \xi^\alpha \mathbf{d}_\alpha(\xi, t) \tag{B.4}$$

is a representation. To deal with cases where (B.4) does not hold, one can add a function to the free energy function that is not obtained by direct integration. The free energy function for a Cosserat rod where (B.4) holds is given by

$$\lambda\psi = \int \rho_o^*\psi^* \, \mathrm{d}A. \tag{B.5}$$

Performing this integration and using, from O'Reilly (1998),

$$\epsilon_{11} = \frac{1}{2}\gamma_{11}, \quad \epsilon_{22} = \frac{1}{2}\gamma_{22}, \quad \epsilon_{33} = \gamma_{33} + \zeta^\alpha\kappa_{\alpha 3}, \tag{B.6}$$

$$\epsilon_{12} = \frac{1}{2}\gamma_{12}, \quad \epsilon_{13} = \gamma_{13} + \frac{1}{2}\zeta^\alpha\kappa_{\alpha 1}, \quad \epsilon_{23} = \gamma_{23} + \frac{1}{2}\zeta^\alpha\kappa_{\alpha 2}, \tag{B.7}$$

we find

$$\begin{aligned}2\lambda\psi = &\frac{1}{4}Ah_{11}\gamma_{11}^2 + \frac{1}{4}Ah_{11}\gamma_{22}^2 + \frac{1}{4}Ah_{11}\gamma_{33}^2 + \frac{1}{2}Ah_{12}\gamma_{11}\gamma_{22} + \frac{1}{2}Ah_{12}\gamma_{11}\gamma_{33} + \frac{1}{2}Ah_{12}\gamma_{22}\gamma_{33} + Ah_{44}\gamma_{12}^2\\ &+ Ah_{44}\gamma_{13}^2 + Ah_{44}\gamma_{23}^2 + \frac{1}{2}I_{11}h_{44}\kappa_{11}^2 + \frac{1}{2}I_{11}h_{44}\kappa_{12}^2 + \frac{1}{2}I_{11}h_{11}\kappa_{13}^2 + \frac{1}{2}I_{22}h_{44}\kappa_{21}^2 + \frac{1}{2}I_{22}h_{44}\kappa_{22}^2\\ &+ \frac{1}{2}I_{22}h_{11}\kappa_{23}^2 - \frac{1}{2}Am_{11}\gamma_{11}\theta - \frac{1}{2}Am_{11}\gamma_{22}\theta - \frac{1}{2}Am_{11}\gamma_{33}\theta - \frac{1}{2}Ac\theta^2 - \frac{1}{2}I_{11}c\theta_1^2 - \frac{1}{2}I_{22}c\theta_2^2\\ &- I_{11}m_{11}\kappa_{13}\theta_1 - I_{22}m_{11}\kappa_{23}\theta_2,\end{aligned} \tag{B.8}$$

where A is the area of the cross-section and $I_{\alpha\alpha}$ are the areal moments of inertia. Thus, by comparison with (19) we find the following coefficients for homogeneous deformations:

$$k_1 = k_2 = k_3 = \frac{1}{4}Ah_{11}, \tag{B.9}$$

$$k_7 = k_8 = k_9 = \frac{1}{2}Ah_{12}, \tag{B.10}$$

$$k_4 = \bar{k}_5 = \bar{k}_6 = Ah_{44}, \tag{B.11}$$

$$k_{18} = -\frac{1}{2}Ac, \quad k_{19} = -\frac{1}{2}I_{11}c, \quad k_{20} = -\frac{1}{2}I_{22}c, \tag{B.12}$$

$$k_{21} = k_{22} = k_{23} = -\frac{1}{2}Am_{11}, \quad k_{24} = -I_{11}m_{11}, \quad k_{25} = -I_{22}m_{11}. \tag{B.13}$$

We have denoted k_5 and k_6 with an overbar because these will not be the final values we use.

As was noted previously, the results (B.9)–(B.13) hold only for deformations where (B.4) holds. This approximation will not hold for transverse bending deformations, so we will improve our approximations of k_5 and k_6 by comparison with exact solutions for a cantilevered linearly elastic rod subject to a transverse end load. This comparison was performed for a rod with orthotropic symmetry and a circular cross-section by Green and Naghdi (1979). We extend their results to include rectangular cross-sections. For any geometry, the coefficient values they found are

$$k_5 = -I_{22}\Big/\frac{\partial\chi(0,0)}{\partial y}, \quad k_6 = -I_{11}\Big/\frac{\partial\Phi(0,0)}{\partial x}, \tag{B.14}$$

where Φ and χ solve the harmonic equations,

$$\Delta\Phi = 0, \quad \Delta\chi = 0, \tag{B.15}$$

subject to boundary conditions dependent on the material properties and the geometry of the cross-section. For our problem, the boundary conditions are; for $y = \pm\frac{h}{2}$,

$$\begin{aligned}\frac{\partial\Phi}{\partial y} &= \mp(s_{1122} + 4s_{1212})\frac{h}{2}x,\\ \frac{\partial\chi}{\partial y} &= -\left(\frac{3}{2}s_{1122} + 2s_{1212}\right)x^2 + \frac{h^2}{8}s_{1122},\end{aligned} \tag{B.16}$$

and, for $x = \pm\dfrac{w}{2}$,

$$\begin{aligned}\frac{\partial\Phi}{\partial x} &= -\left(\frac{3}{2}s_{1122} + 2s_{1212}\right)y^2 + \frac{w^2}{8}s_{1122},\\ \frac{\partial\chi}{\partial x} &= \mp(s_{1122} + 4s_{1212})\frac{w}{2}y.\end{aligned} \tag{B.17}$$

The compliances s_{ijkl} are defined by the identities

$$s_{ijkl}c_{mnij} = \frac{1}{2}(\delta^m_k\delta^n_l + \delta^m_l\delta^n_k), \tag{B.18}$$

and have the same symmetry properties as c_{ijkl}. Using (B.2), we find,

$$\begin{aligned} s_{1111} &= s_{2222} = s_{3333} = \frac{h_{11}+h_{12}}{(h_{11}+2h_{22})(h_{11}-h_{12})}, \\ s_{1122} &= s_{1133} = s_{2233} = \frac{h_{12}}{(h_{11}+2h_{22})(h_{12}-h_{11})}, \\ s_{1212} &= s_{1313} = s_{2323} = \frac{1}{4h_{44}}, \end{aligned} \tag{B.19}$$

when (B.18) is solved for a cubic crystal.

We solve the boundary-value problems (B.15)–(B.17) by using the method outlined in Love (1927). This yields the following equations for the bending coefficients:

$$\begin{aligned} k_5 &= Ah_{44}\left(\frac{3}{2} + \frac{h_{12}h_{44}}{(h_{11}+2h_{12})(h_{12}-h_{11})}\left(\frac{w^2}{h^2} + \frac{12w^2}{\pi^2h^2}\sum_{n=1}^{\infty}\frac{(-1)^n}{n^2}\operatorname{sech}\frac{n\pi h}{w}\right)\right)^{-1}, \\ k_6 &= Ah_{44}\left(\frac{3}{2} + \frac{h_{12}h_{44}}{(h_{11}+2h_{12})(h_{12}-h_{11})}\left(\frac{h^2}{w^2} + \frac{12h^2}{\pi^2w^2}\sum_{n=1}^{\infty}\frac{(-1)^n}{n^2}\operatorname{sech}\frac{n\pi w}{h}\right)\right)^{-1}. \end{aligned} \tag{B.20}$$

In a classical setting, we would take

$$k_5 = k^1\bar{k}_5, \quad k_6 = k^2\bar{k}_6, \tag{B.21}$$

where k^α are known as the Timoshenko shear correction factors. Comparing these values for k_5 and k_6 with the values in (B.20) we find a formula for the correction factors.

The remaining coefficients are determined by comparison with the results found by Green and Naghdi (1979). Substituting our material properties, (B.2), (B.19) and (23), results in the coefficients (24). Thus, we have prescriptions for all 25 constants in the strain energy function of a material with cubic symmetry in terms of the three mechanical material parameters, the thermal material parameters, and the geometry of the rod.

For the example of crystalline silicon, we use values for the specific heats and thermal expansion coefficients given in table form as a function of temperature from Kagaya and Soma (1999) and Soma and Kagaya (1999) respectively. And, from George (1999) we use values for the elastic material parameters. At standard temperature and pressure, they are

$$\begin{aligned} h_{11} &= 1.6564 \times 10^{11}\ \text{Pa}, \\ h_{12} &= 0.6394 \times 10^{11}\ \text{Pa}, \\ h_{44} &= 0.7951 \times 10^{11}\ \text{Pa}. \end{aligned} \tag{B.22}$$

In addition, we have the following temperature dependence for silicon,

$$\begin{aligned} \left(\frac{1}{h_{11}}\right)\frac{\mathrm{d}h_{11}}{\mathrm{d}T} &= -9.4 \times 10^{-5}\ \text{K}^{-1}, \\ \left(\frac{1}{h_{12}}\right)\frac{\mathrm{d}h_{12}}{\mathrm{d}T} &= -9.8 \times 10^{-5}\ \text{K}^{-1}, \\ \left(\frac{1}{h_{44}}\right)\frac{\mathrm{d}h_{44}}{\mathrm{d}T} &= -8.3 \times 10^{-5}\ \text{K}^{-1}. \end{aligned} \tag{B.23}$$

We now have full prescriptions for the constitutive equations for a rod of crystalline silicon that is initially straight and prismatic.

References

Beeby, S.P., Ensell, G., Baker, B.R., Tudor, J., White, N.M., 2000. Micromachined silicon resonant strain gauges fabricated using SOI wafer technology. Journal of Microelectromechanical Systems 9, 104–111.

Bragg, S.W.L., Claringbull, G.F., 1965. The Crystalline State. Crystal Structures of Minerals, vol. IV. Cornell University Press, Ithaca, NY.

Carlson, D.E., 1972. Linear thermoelasticity. In: Truesdell, C., (Ed.), Handbuch der Physik, vol. VIa/2.

EerNisse, E.P., 1980. Miniature quartz resonator force transducer. US Patent 4 215 570.

George, A., 1999. Elastic constants and moduli of diamond cubic Si. In: Hull, R., (Ed.), Properties of Crystalline Silicon. pp. 98–103.

Green, A.E., Naghdi, P.M., 1979. On thermal effects in the theory of rods. International Journal of Solids and Structures 15, 829–853.

Green, A.E., Naghdi, P.M., 1995. A unified procedure for the construction of theories of deformable media. II. Generalized continua. Proceedings of the Royal Society of London A 448, 357–377.

Green, A.E., Naghdi, P.M., Wenner, M.L., 1974. On the theory of rods. II. Developments by direct approach. Proceedings of the Royal Society of London A 337, 485–507.

Gurtin, M.E., 1972. The linear theory of elasticity. In: Truesdell, C. (Ed.), Handbuch der Physik, vol. VIa/2.

Hutchinson, J.R., 2001. Shear coefficients for Timoshenko beam theory. Journal of Applied Mechanics 68, 87–92.

Kagaya, H., Soma, T., 1999. Specific heats of c-Si and molten Si. In: Hull, R., (Ed.), Properties of Crystalline Silicon, pp. 153–154.

Kawashima, H., 1996. The shear coefficient for quartz crystal of rectangular cross section in Timoshenko's beam theory. IEEE Transactions on Ultrasonics, Ferroelectronics and Frequency Control 43 (3), 434–440.

Kinkaid, N.M., O'Reilly, O.M., 2002. Pulling apart a press-fitted joint. Mathematics and Mechanics of Solids 7, 307–318.

Love, A.E.H., 1927. A Treatise on the Mathematical Theory of Elasticity, fourth ed. Cambridge University Press, Cambridge.

Luo, C., O'Reilly, O.M., 2000. On the material symmetry of elastic rods. Journal of Elasticity 60, 35–53.

Naghdi, P.M., 1982. Finite deformations of elastic rods and shells. In: Carlson, D.E., Shields, R.T. (Eds.), Proceedings of the IUTAM Symposium on Finite Elasticity, Bethlehem, PA. Martinus Nijhoff, The Hague, pp. 47–104.

O'Reilly, O.M., 1998. On constitutive relations for elastic rods. International Journal of Solids and Structures 35, 1009–1024.

O'Reilly, O.M., Turcotte, J.S., 1996. Another mode of vibration in a Timoshenko beam. Journal of Sound and Vibration 198, 517–521.

Puchegger, S., Loidl, D., Kromp, K., Peterlik, H., 2003. Hutchinson's shear coefficient for anisotropic beams. Journal of Sound and Vibration 266 (2), 207–216.

Rubin, M.B., 2000. Cosserat Theories: Shells, Rods, and Points. Kluwer Academic Publishers, Boston.

Soma, T., Kagaya, H., 1999. Thermal expansion coefficients of c-Si. In: Hull, R. (Ed.), Properties of Crystalline Silicon. pp. 153–154.

Wojciechowski, K.E., Boser, B.E., Pisano, A.P., 2004. A MEMS resonant strain sensor operated in air. In: Proceedings of the 17th IEEE International Conference on Micro Electro Mechanical Systems. MEMS 2004, Maastricht, The Netherlands. pp. 841–845.

Zheng, Q., 1994. Theory of representations for tensor functions—a unified invariant approach to constitutive equations. ASME Applied Mechanics Reviews 47, 545–587.